C. R. Geoscience 342 (2010) 837–846

Contents lists available at ScienceDirect

Comptes Rendus Geoscience

www.sciencedirect.com

Petrology, geochemistry

^{40}Ar-^{39}Ar Geochronology in a gneiss dome within the Zagros Orogénic Belt

Géochronologie ^{40}Ar-^{39}Ar dans un dôme gneissique de la ceinture orogénique du Zagros

Akram Alizadeh [a,*], Margarita López Martínez [b], Khalil Sarkarinejad [c]

[a] *Department of Geology, Faculty of Sciences, Urmia University, Urmia 57153-165, Iran*
[b] *Department of Geology, CICESE (Centro de Investigación Científica y de Educación Superior de Ensenada), Baja California, Mexico*
[c] *Department of Earth Sciences, College of Sciences, Shiraz University, Shiraz 71454, Iran*

ARTICLE INFO

Article history:
Received 19 January 2009
Accepted after revision 27 July 2010
Available online 25 October 2010

Presented by Jean Auboin

Keywords:
Neo-Tethys
^{40}Ar-^{39}Ar geochronology
Zagros
Gneiss dome
Iran

ABSTRACT

Exhumation of the Tutak mantled gneiss dome without significant cooling has taken place in a doubly plunging anticline within the Sanandaj-Sirjan HP-LT metamorphic belt in the Zagros Thrust System of Iran. Reconstruction of structural evolution of the Tutak gneiss dome at the contact between Arabian and Iranian plates by ^{40}Ar/^{39}Ar geochronology exhibits history of the closure of Neo-Tethyan Ocean. There are two granites of different ages in the core of dome; the oldest corresponds to the central Iranian continental crust and was deformed at about 180 Ma. The younger granite was emplaced in the NE–SW transpression system. The timing of strain-related fabrics and exhumation history of the region illustrates the closure of Neo-Tethys and beginning of continent-continent collision at about 77 Ma, as constrained by a well defined plateau ^{40}Ar/^{39}Ar age obtained on biotite. Then, the biotite age corresponds to the second stage of emplacement of the Bendenow granite-gneiss which illustrating repeated orogenic events. Continuing deformation without interruption that by now has been created at about 77 Ma, was largely restricted to the transpression and high proportion of simple shear components relative to the pure shear components along the NE–SW.

Mots clés :
Néo-Téthys
Géochronologie ^{40}Ar-^{39}Ar
Zagros
Dôme gneissique
Iran

RÉSUMÉ

L'exhumation du dôme gneissique mantellique de Tutak sans refroidissement significatif a pris place dans un anticlinal plongeant doublement au sein de la ceinture métamorphique HP-LT de Sanandaj-Sirjan dans le système charrié du Zagros en Iran. La reconstitution de l'évolution structurale du dôme gneissique de Tutak au contact entre les plaques Arabique et Iranienne par géochronologie ^{40}Ar/^{39}Ar montre l'histoire de la fermeture de l'Océan néo-téthysien. On observe deux granites différents au cœur du dôme; le plus ancien correspond à la croûte continentale centro-iranienne et a été déformé vers 180 Ma. Le plus jeune est situé dans le système de transgression NE–SW. La période d'édification liée à la déformation et l'histoire de l'exhumation de la région illustre la fermeture de la Néo-Téthys et le commencement de la collision continent-continent à environ 77 Ma, contraint par un plateau d'âge ^{40}Ar/^{39}Ar bien définis, obtenu sur biotite. L'âge de la biotite correspond alors à la seconde étape de mise en place du gneiss-granite de Bendenow qui illustre des évènements orogéniques répétés. La déformation qui a débuté vers 77 Ma et

* Corresponding author.
E-mail addresses: ak.alizadeh@urmia.ac.ir, alizadeh.akram@yahoo.com (A. Alizadeh), marlopez@cicese.mx (M. López Martínez), sarkarinejad@geology.susc.ac.ir (K. Sarkarinejad).

1631-0713/$ – see front matter © 2010 Académie des sciences. Published by Elsevier Masson SAS. All rights reserved.
doi:10.1016/j.crte.2010.07.005

s'est poursuivie jusqu'à présent, a été nettement réduite à la transpression et à une forte proportion de composants de simple cisaillement par rapport aux composants de pur cisaillement selon une direction NE–SW.

1. Introduction

The Zagros Suture Zone of Iran is a part the Alpine-Himalayan mountain chain formed on the northern Arabian plate margin (Alavi, 1994) as the Neo-Tethys closed in the Early to Middle Eocene (Ghasemi and Talbot, 2006). The Zagros fold and thrust belt that lie on the northeastern margin of the Arabian platform (Sepehr and Cosgrove, 2004) consists of a Phanerozoic succession with a stratigraphic thickness of up to 10 km that is folded into kilometer-scale simple anticlines and synclines (Stocklin, 1968) and extends for about 2000 km in the NW–SE direction from the eastern Turkey to the Oman line in southern Iran. The Sanandaj-Sirjan metamorphic belt (Sarkarinejad, 2007; Sarkarinejad and Azizi, 2008) within the Zagros Orogenic Belt, extends 1500 km long and 100 km wide (Mohajjel et al., 2003), and is characterized by metamorphism and obliquely thrust wedge with asymmetrical structures in the HP-LT metamorphic rocks (Sarkarinejad and Azizi, 2008).

Orogenic belts commonly display locally exhumed high-grade rock termed gneiss domes or metamorphic core complexes that reflect a variety of tectonic settings (e.g., extension, compression, buoyancy-driven plutonism) (Amato et al., 1994; Getty and Gromet, 1992). Such features are composed of metamorphic and plutonic rocks metamorphosed at amphibolite to granulite facies conditions during the latter stages of orogenesis (Schneider et al., 2001).

The Tutak gneiss dome within the Sanandaj-Sirjan HP-LT metamorphic belt in the Zagros suture zone is a good example to study the deformation and repeated orogenic events because it is part of the continental-scale of transpression between the Arabia and central Iran platforms. The Tutak gneiss dome represents the culmination of metamorphism between the carbonate shelf (Zagros Orogenic Belt) and Urmia-Dokhtar Magmatic Arc (Fig. 1). It has a large number of well-exposed asymmetrical structures. Reconstruction of structural history of the Tutak gneiss dome is complementary with its dating and is

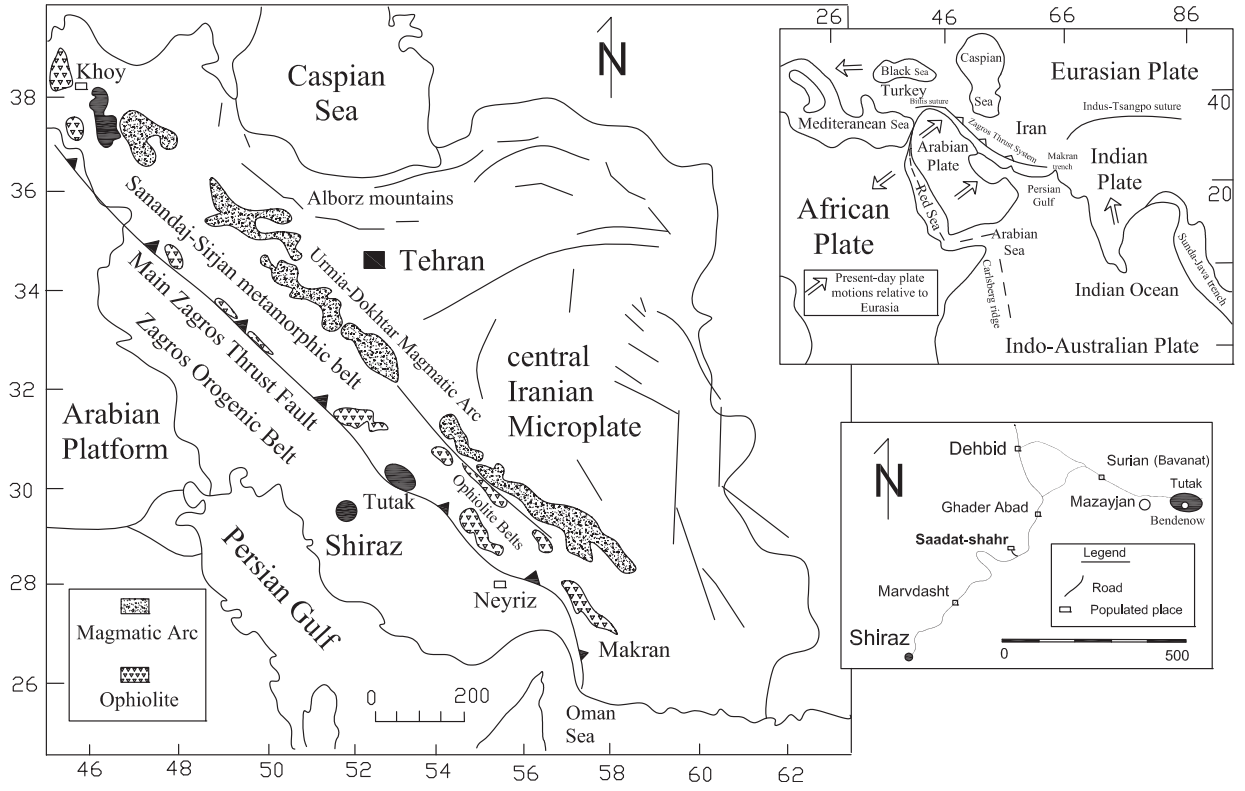

Fig. 1. Geographic map and some main tectonic features of Iran. The studied area is located within the Sanandaj-Sirjan metamorphic belt, between the Zagros Thrust System and Urmia-Dokhtar Magmatic Arc.

Fig. 1. Carte géographique et quelques uns des principaux traits tectoniques de l'Iran. La zone étudiée se situe au sein de la ceinture métamorphique entre le système de charriage du Zagros et l'arc magmatique Urmia-Dokhtar.

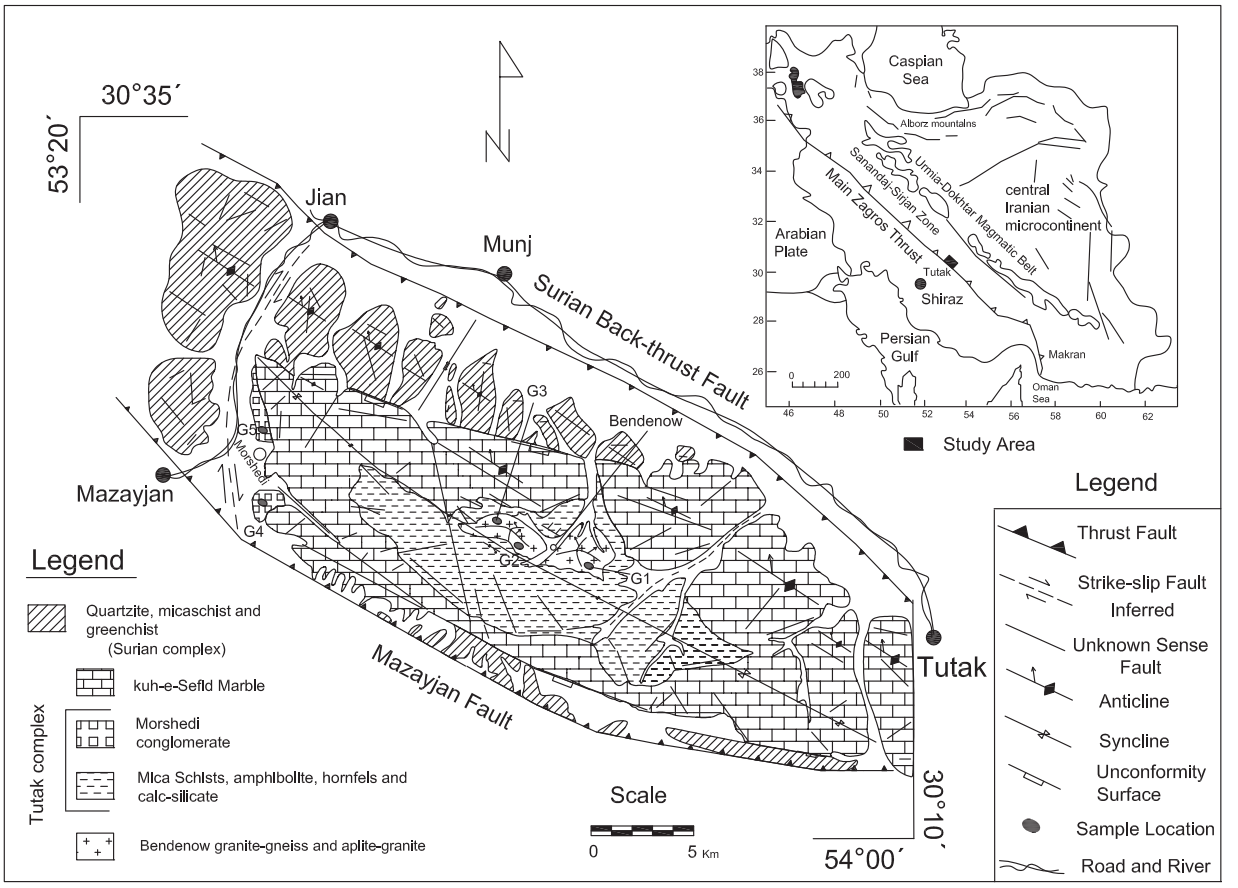

Fig. 2. Geological map of the Tutak gneiss dome. The two major faults, Surian at the north and Mazayjan at the south sandwiched the dome and aligned the Zagros Thrust System.

Fig. 2. Carte géologique du dôme gneissique de Tutak. Les deux principales failles, Surian au nord et Mazayan au sud prennent le dôme « en sandwich » et alignent le système de charriage de Zagros.

the aim of the present work. Detailed description of the tectonic events are presented and discussed in the following section. The new results presented here, favor demise of the Neo-Tethyan Ocean versus forming the Zagros Orogenic Belt.

2. Geological framework

Gneiss domes are typically bounded by shear zones that accommodated differential exhumation relative to their surrounding host rocks (Whitington, 2004). Two shear zones are present; the Surian as an antithetic back-thrust fault at the north and Mazayjan synthetic thrust fault at the south bound the dome, which is aligned along the Zagros Thrust System (Sarkarinejad and Alizadeh, 2009; Sarkarinejad et al., 2008 Fig. 2). At the northwest of the Tutak gneiss dome these two faults join and form the Dehbid thrust fault (Houshmand-Zadeh et al., 1990). So, the Dehbid shear zone along the Main Zagros Thrust Fault is a ductile north-east-verging shear zone with dextral sense of shear and combination of two Surian and Mazayjan faults, define a crustal-scale antiformal pop-up structure that exhumed the dome within a bivergent wedge (Sarkarinejad and Alizadeh, 2009).

Throughout the zone are present the Surian complexes (quartzite, greenschist and micaschist), tens to hundreds of meters thick marbles (Kuh-e-Sefid), Tutak complex (micaschist, amphibolite, hornfels and meta-conglomerate) and two types of granite. The Tutak gneiss dome is 10 to 20 km long (Fig. 2). Its core consists of the aplite-granite and Bendenow granite-gneiss, is mantled by the Silurian and Devonian Tutak metasedimentary complex and a thick bed of marbles (Fig. 2). They are in turn unconformably overlain by the Permian Surian complex (Houshmand-Zadeh et al., 1990).

The foliation generally dips away from the Tutak pluton in the core of the dome with shallow dips on the flanks of the dome. The attitude of foliation as indicated by the results of measurements in the scattered outcrops of gneisses, greenschists, and micaschists is different around the Tutak gneiss dome.

Table 1 shows the major and trace element of the granites inside the dome. The quartz and feldspar are the dominant minerals in aplite-granite. The Bendenow granite-gneiss is coarse-grained, strongly to weakly

Table 1
Major and trace element of the rocks of the Tutak gneiss dome. G_1, G_2 and G_3, define the Bendenow granite-gneiss; G_4 and G_5 illustrate aplite-granite.

Tableau 1
Elements majeurs et éléments trace des roches du dôme gneissique de Tutak. G_1, G2 et G_3 correspondent au gneiss-granite de Bendenow, G_4 et G_5 au granite-aplite.

Composite	G_1	G_2	G_3	G_4	G_5
SiO_2	70.0	73.57	64.0	71.13	76.3
Al_2O_3	18.84	14.05	19.52	14.23	8.2
Fe_2O_3	1.34	3.23	3.73	3.67	2.78
MgO	0.19	0.90	2.14	1.34	1.0
CaO	0.71	1.05	3.0	1.71	3.84
Na_2O	4.7	3.21	5.97	2.82	3.78
K_2O	1.84	2.39	1.46	4.19	1.46
P_2O_5	<0.02	0.18	0.13	0.07	0.10
FeO	1.226	2.907	3.33	3.303	3.051
Element					
Rb	228	114	175	378	272
Sr	84	137	272	147	175
K/Rb	203	209.6	156.6	111	138
K/Ba	12.18	34.3	67.6	44.4	59.5
Rb/Sr	2.714	0.832	1.534	2.57	1.554
Ca/Sr	84.5	76.6	88.6	116.3	97.7
Cr	3	18	23	31	19
Ni	<5	<5	<5	9	9
V	13	37	53	60	47
Co	5	5.5	6	3	7
Cu	3	27	11	2	4
Ni/Co	<1	<0.9	<0.8	3	1.285

foliated gneiss, composed of phenocrysts of K-feldspar, and biotite, with accessory garnet.

The Tutak gneiss dome is a structural window of metamorphic complex in the Zagros Orogenic Belt that formed in the suture zone during collision of the African-Arabian continent and Iranian microcontinent. It is situated between two ophiolite belts; Khoy-Neyriz and Naien-Baft (Ghasemi and Talbot, 2006; Fig. 1). The Tutak and Surian complexes inside the Tutak gneiss dome have been metamorphosed at least in two phases of deformation. Most deformation in the Dehbid shear zone took place under amphibolite-facies conditions. A later deformation under greenschist facies conditions resulted in retrogression, greenschist ultramylonite, and the formation of extensive chloritic breccia localized at the top of the shear zone (Alizadeh, 2008).

3. ^{40}Ar-^{39}Ar geochronology

To constrain and date the fabric development during the formation of the orogenic belts, we performed ^{40}Ar-^{39}Ar step-heating experiments on the Bendenow granite-gneiss (Biotite 1a) and aplite-granite (Biotite 2a, Muscovite 2a and Muscovite 2aa) samples (Fig. 2; sample location). These samples are representative of pre- and syn-deformational granites from the Tutak gneiss dome. The ^{40}Ar-^{39}Ar analyses were performed at CICESE (Centro de Investigación Científica y de Educación Superior de Ensenada) Geochronology Laboratory using a VG5400 mass spectrometer and a Coherent Innova 70 Laser to heat the samples.

3.1. Sample description

Thin sections of the samples were examined to select the best minerals available for ^{40}Ar-^{39}Ar dating. The mineral separation was performed at the CICESE's Geochronology Laboratory. The samples were crushed, sieved and washed in distilled water. To concentrate the minerals of interest a Frantz magnetic separator was used. Finally the minerals were prepared by hand picking under the binocular microscope. Care was taken to insure that the biotite and muscovite concentrates were free of alteration. The minerals were irradiated at the Uranium enriched research reactor of McMaster University in position 5C using Cd liner. As irradiation monitor, sanidine TCR 2 of 27.87 ± 0.04 Ma was used. The argon isotopes were corrected for blank, decay of ^{37}Ar and ^{39}Ar, mass discrimination and interference reactions of Ca, K and Cl. All errors reported are 1σ. The decay constants recommended by Steiger and Jäger (1977) were used in the age calculations. Whenever it applies, the equations given by York et al. (2004) were used to calculate the best straight line. With the exception of within spectra errors, the integrated, plateau and isochron ages include the uncertainty in the irradiation monitor J.

3.2. Results

The results obtained for aplite-granite Muscovite 2a and Muscovite 2aa are given in Fig. 3 and Table 2. Biotite 1a from the Bendenow granite-gneiss and Biotite 2a from the aplite-granite are presented in Fig. 4 and Table 3. Muscovite sample 2aa was step-heated with the argon released in 9 fractions. The first part of the age spectrum (Fig. 3a) yielded unrealistic old ages indicating the presence of excess argon. Then some argon loss is indicated by age less or equal to 153 Ma on two fractions, these represent ~30% of the ^{39}Ar released. The last five fractions fulfill the criteria for plateau age: all but one of the ages for these fractions are in agreement within 1σ, additionally these fractions represent more than 50% of the ^{39}Ar

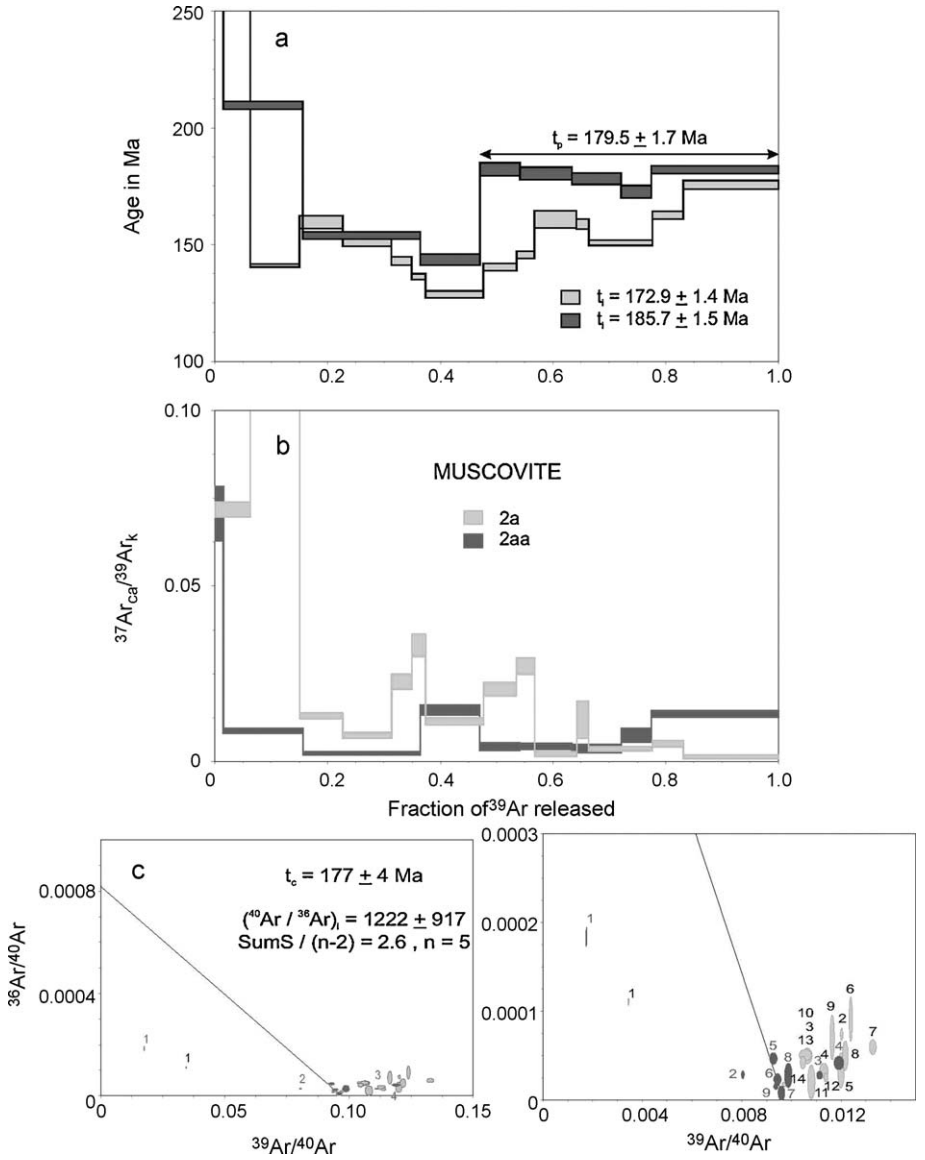

Fig. 3. ^{40}Ar-^{39}Ar results for the aplite-granite (Muscovite 2a and 2aa). a: Age spectra obtained, the arrows identify the plateau fractions. The integrated age and plateau age are given, these are 1σ and include the uncertainty in J; b: The $^{37}Ar_{Ca}/^{39}Ar_K$ diagram indicates slight variation in the ratio for the muscovite; c: Correlation $^{36}Ar/^{40}Ar$ versus $^{39}Ar/^{40}Ar$ diagram. The isochron ages were calculated using the plateau fractions of the micas; the equations given in York et al. (2004) were used to calculate the best straight line. The line plotted with the plateau fractions of the biotite was forced trough $(^{40}Ar/^{36}Ar)_i = 295.5$.

Fig. 3. Résultats ^{40}Ar-^{39}Ar pour le granite-aplite (muscovite 2a et 2aa). a: spectres d'âge obtenus; les flèches identifient les fractions plateau. Âge intégré et âge plateau sont fournis avec une erreur de 1 σ et comportent l'incertitude en J; b: Le diagramme $^{37}Ar_{Ca}/^{39}Ar_K$ indique une légère variation dans le rapport pour la muscovite; c: Diagramme de corrélation $^{36}Ar/^{40}Ar$. Les âges isochrone ont été calculés en utilisant les fractions plateau; les équations utilisées in York et al. (2004) ont été utilisées pour calculer la meilleure ligne droite possible. La ligne obtenue à partir des fractions plateau de la biotite a été forcée pour $(^{40}Ar/^{36}Ar) = 295{,}5$.

released. The weighted mean of the individual ages of these five fractions yielded a plateau age of 179.5 ± 1.7 Ma. In the correlation diagram (Fig. 3c) the inverse of the y-intercept of the isochron calculated with plateau fractions indicates a $(^{40}Ar/^{36}Ar)_i = 1222$ confirming the presence of excess argon. Since the ^{40}Ar of the plateau fractions consists of almost pure radiogenic argon, the effect of excess argon in them is negligible, thus yielding an isochron age of 176.9 ± 3.9 Ma, which is statistically undistinguishable from the plateau age. Muscovite sample 2a behaved in a similar manner as Muscovite 2aa. A more detailed experiment was performed with this sample since 14 fractions were collected. Again the age spectrum (Fig. 3a) displays old ages for the first fractions followed by low ages, but in this case the shape of the age spectrum indicates a more pronounced argon loss. The plateau of Muscovite 2aa is defined by the fractions released with a laser power of greater or equal to 0.68 Watts. The ages obtained on Muscovite 2a for the argon released applying similar laser power, range between 140 and 160 Ma, displaying an up and down staircase pattern that climbs to

Table 2
Summary of the Muscovite laser step-heating ^{49}Ar-^{39}Ar results. The decay constants given in Steiger and Jäger (1977) were used in the data reduction. All errors are 1σ. Within spectra errors do not include the error in J. The integrated age includes the uncertainty in J.

Tableau 2
Résultats ^{49}Ar-^{39}Ar du chauffage par palier au laser de la muscovite. Les constantes de désintégration fournies par Steiger et Jäger (1977) ont été utilisées dans la réduction des données. Toutes les erreurs sont données en 1σ. L'erreur en J n'est pas incluse dans les spectres d'erreur. L'âge intégré comporte l'incertitude en J.

Sample	Pwr[a]	F^{39}Ar	$^{39}Ar_{cum}$	Age in Ma	%$^{40}Ar_{atm}$	%$^{40}Ar^{*}$	$^{37}Ar_{Ca}/^{39}Ar_{K}$
Muscovite 2a	0.30	0.0628	0.0628	446.7 ± 2.1	3.27	96.73	0.072
	0.35	0.0872	0.1500	141.0 ± 0.7	2.19	97.81	0.249
	0.40	0.0766	0.2266	159.6 ± 2.7	1.47	98.53	0.013
	0.45	0.0870	0.3136	151.5 ± 2.2	0.97	99.03	0.007
	0.50	0.0361	0.3497	143.0 ± 1.7	0.98	99.02	0.023
	0.55	0.0244	0.3741	136.4 ± 1.3	2.70	97.30	0.033
	0.62	0.1026	0.4767	128.8 ± 1.4	1.76	98.24	0.011
	0.67	0.0585	0.5351	140.4 ± 1.5	1.47	98.53	0.021
	0.72	0.0321	0.5672	145.6 ± 1.5	2.09	97.91	0.027
	0.79	0.0747	0.6419	160.8 ± 3.7	1.50	98.50	0.002
	0.80	0.0218	0.6637	158.8 ± 2.2	0.59	99.41	0.012
	1.20	0.1132	0.7769	150.7 ± 1.1	0.75	99.25	0.004
	1.50	0.0545	0.8313	162.6 ± 1.7	1.25	98.75	0.005
	3.00	0.1687	1.0000	175.5 ± 1.8	0.52	99.48	0.001
Muscovite 2aa	0.20	0.0150	0.0150	779.6 ± 8.3	5.43	94.57	0.071
	0.40	0.1414	0.1564	209.6 ± 1.6	0.84	99.16	0.009
	0.50	0.2078	0.3641	153.9 ± 1.6	0.83	99.17	0.002
	0.55	0.1060	0.4702	143.6 ± 2.3	1.23	98.77	0.015
	0.68	0.0709	0.5411	182.2 ± 2.8[b]	1.38	98.62	0.004
	0.85	0.0924	0.6335	180.4 ± 2.7[b]	0.69	99.31	0.004
	1.05	0.0877	0.7212	178.2 ± 2.5[b]	0.24	99.76	0.004
	1.40	0.0531	0.7742	172.6 ± 2.6[b]	0.82	99.18	0.007
	3.00	0.2258	1.0000	182.0 ± 1.7[b]	0.45	99.55	0.014

Sample	^{39}Ar	$^{40}Ar^{*}/^{39}Ar_{K}$	Age in Ma	$^{37}Ar_{Ca}/^{39}Ar_{K}$	%$^{40}Aratm$	%$^{40}Ar^{*}$	$^{40}Ar/^{36}Ar$
Muscovite 2a	7.855E-03	32.39 ± 0.12	172.8 ± 1.4	0.03	1.59	98.41	18529.6
Muscovite 2aa	5.198E-03	34.93 ± 0.16	185.7 ± 1.5	0.01	1.12	98.88	26495.0

J = 0.003104 ± 0.000023.
[a] Power in watts applied to release the argon isotopes.
[b] Plateau fractions.

175 Ma on the last fraction, an age close to the plateau age defined by Muscovite 2aa. The $^{37}Ar_{Ca}/^{39}Ar_{K}$ diagram (see Fig. 3b) indicates that the Ca/K ratio of these muscovites is slightly different, which may explain the different behaviors between these micas with respect to their argon retentivity, muscovite 2aa displaying a less disturbed pattern than muscovite 2a on this diagram.

A very detailed step-heating experiment was performed on Biotite 1a, with a total of 24 fractions collected (Fig. 4). An extensive plateau is observed for this sample. The first part of the age spectrum (see Fig. 4a) indicates slight argon loss; however, twenty one consecutive fractions, which represent 88% of the ^{39}Ar released, yielded ages statistically undistinguishable within 1σ. The weighted mean of their individual ages yielded a plateau age of 76.8 ± 0.2 Ma. In the correlation diagram (Fig. 4c) the plateau fractions cluster around a point close to the abscissa axis. This distribution does not define an isochron line. The 76.7 ± 1.2 Ma age displayed on the correlation diagram (Fig. 4c) was calculated with the plateau fractions of Biotite 1a and a y-intercept through $(^{40}Ar/^{36}Ar)_{i} = 295.5$; this is equivalent to assume that the non radiogenic ^{40}Ar is of atmospheric composition. The best estimate for the age of Bendenow granite-gneiss is thus taken from the plateau age of 76.8 ± 0.2 Ma of Bitotite 1a. The other biotite analyzed comes from the aplite-granite, biotite 2a sample, on which a less detailed experiment was conducted; only 10 fractions were collected. The integrated age obtained on Biotite 1a is statistically undistinguishable from the integrated age of Biotite 2a with values of 72.9 ± 0.6 Ma and 72.4 ± 0.6 Ma respectively. However, Biotite 2a yielded a perturbed age spectrum. It is possible that this biotite was older and its actual age is the product of a resetting event associated to the Bendenow granite-gneiss intrusion.

4. Discussion

4.1. Geodynamics of the Tutak gneiss dome

Material from the partially molten layer may ascend as diapirs if the balance between vertical flow (buoyancy) and lateral flow (thinning/extrusion) allows a diapir to rise to shallow levels without significant cooling (Teyssier and Whitney, 2002). The buoyancy forces arising from thickened crust within the transpression have caused the emplacement of the Bendenow granite-gneiss (Sarkarinejad and Alizadeh, 2009). As shown by Fletcher (1995) and Ramsay (1967), gneiss domes without spatial association of synkinematic plutons could develop by formation of doubly plunging antiforms. The Bendenow granite-gneiss in the core of the Tutak gneiss dome is a synkinematic

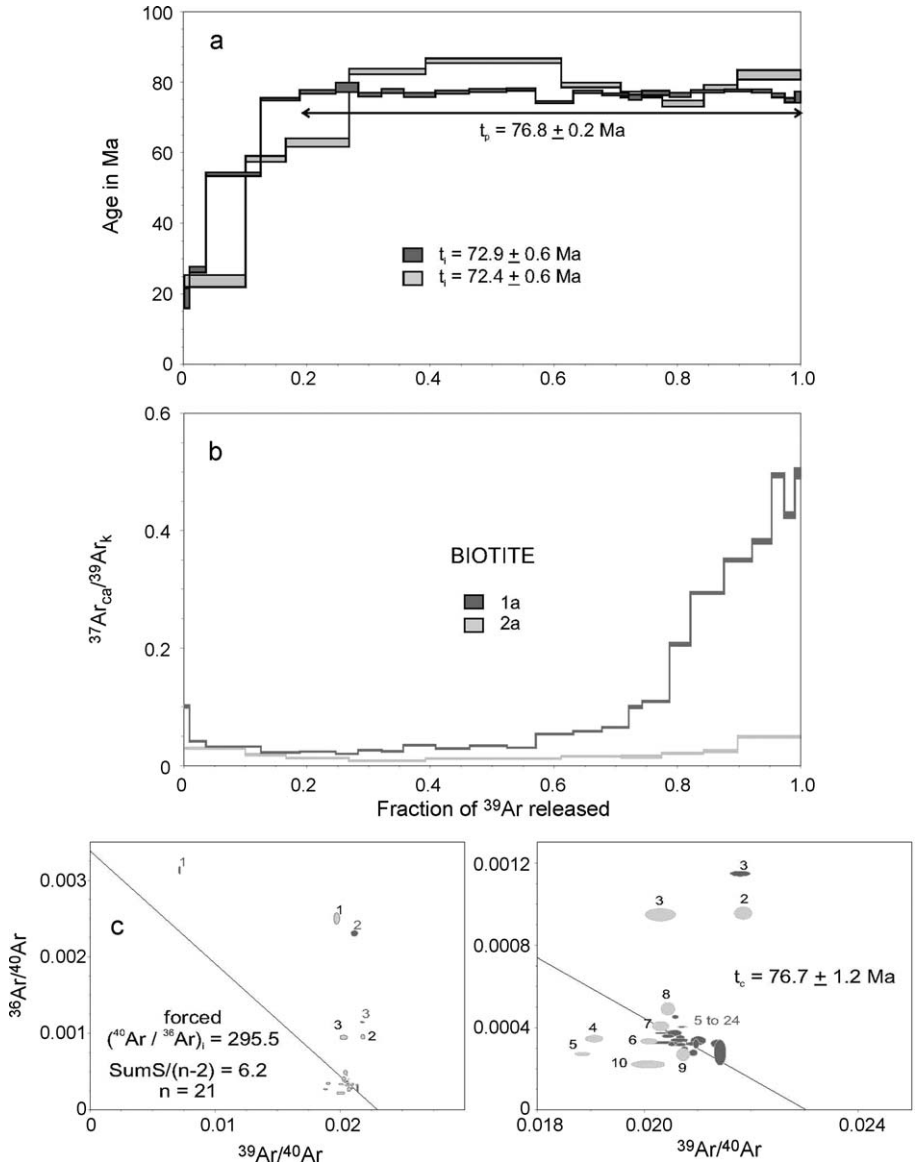

Fig. 4. Age spectra for Biotite 1a (from the Bendenow granite-gneiss) and Biotite 2a (from the aplite-granite) by ^{40}Ar-^{39}Ar geochronology.
Fig. 4. Spectres d'âge pour la biotite 1a (gneiss-granite de Bendenow) et biotite 2a (granite-aplite) par analyse géochronologique ^{40}Ar-^{39}Ar.

batholith that has been emplaced by forming of doubly plunging anticline (Sarkarinejad and Alizadeh, 2009).

Dips are steeper in the north-central part of the range in part because the foliation is locally steeper near the intrusive contact of the pluton (Alizadeh, 2008). The sub-vertical orientation of the foliation in the contact rocks between aplite sub-dome and schists in the Tutak complex is parallel (mimicking the dome shape), to illustrate the injection of aplite-granite pluton into schist facies in the core.

The prograde and retrograde metamorphism in the Tutak gneiss dome has occurred at two stages of conjugate deformations, which are related to the different proportions of pure shear and simple shear components, respectively. During the prolonged stress field of deformation and high temperatures in the feldspar grain of the aplite-granite, plagioclase twining produced lattice misorientation and line dislocations and lattice glide. The orogenic process was reactivated by intrusion of the new compressional granitic magma inside the Tutak complex and metamorphosed the first stage granite (aplite-granite) and new sediments (Alizadeh, 2008).

Thrust up within the sediments, are pieces of the basement. Amphibolite-facies in the Tutak complex originally derived from the basic and ultrabasic rocks of down going metamorphosed oceanic slab so, exhibit a retrograde metamorphism (Nuri, 2005). Later deformation under greenschist facies conditions resulted in retrogression, greenschist ultramylonite, and the formation of extensive chloritic breccia localized at the top of the shear zone.

Table 3
Summary of the Biotite laser step-heating ^{49}Ar-^{39}Ar results. All errors are 1σ. Within spectra errors do not include the error in J. The integrated age includes the uncertainty in J.

Tableau 3
Résultats ^{49}Ar-^{39}Ar du chauffage par palier au laser de la biotite. Toutes les erreurs sont données en 1σ. L'erreur en J n'est pas incluse dans les spectres d'erreur. L'âge intégré comporte l'incertitude en J.

Sample	Pwr[a]	$F^{39}Ar$	$^{39}Ar_{cum}$	Age in Ma	$\%^{40}Ar_{atm}$	$\%^{40}Ar^{*}$	$^{37}ArCa/^{39}Ar_K$
Biotite 1a	0.20	0.0097	0.0097	18.6 ± 2.8	92.59	7.41	0.10
	0.40	0.0268	0.0365	26.8 ± 0.8	68.28	31.72	0.04
	0.70	0.0890	0.1255	53.9 ± 0.5	33.93	66.07	0.03
	0.80	0.0624	0.1879	75.2 ± 0.4[b]	11.91	88.09	0.02
	0.90	0.0586	0.2464	77.3 ± 0.5[b]	11.03	88.97	0.02
	1.00	0.0363	0.2827	78.5 ± 1.3[b]	9.67	90.33	0.02
	1.10	0.0378	0.3206	76.5 ± 0.5[b]	11.14	88.86	0.03
	1.20	0.0359	0.3564	77.5 ± 0.6[b]	9.40	90.60	0.02
	1.35	0.0516	0.4081	76.4 ± 0.6[b]	11.04	88.96	0.03
	1.45	0.0550	0.4631	77.2 ± 0.5[b]	10.60	89.40	0.03
	1.58	0.0606	0.5236	77.6 ± 0.4[b]	9.56	90.44	0.03
	1.70	0.0470	0.5706	77.9 ± 0.4[b]	9.46	90.54	0.03
	1.80	0.0610	0.6316	74.4 ± 0.3[b]	13.36	86.64	0.05
	1.90	0.0464	0.6780	77.3 ± 0.4[b]	9.69	90.31	0.06
	2.00	0.0432	0.7212	76.5 ± 0.4[b]	10.41	89.59	0.06
	2.10	0.0212	0.7424	75.7 ± 0.7[b]	9.96	90.04	0.10
	2.45	0.0447	0.7871	76.9 ± 0.6[b]	10.03	89.97	0.11
	2.80	0.0345	0.8216	76.4 ± 0.6[b]	9.49	90.51	0.21
	3.30	0.0543	0.8759	77.4 ± 0.4[b]	9.37	90.63	0.29
	3.80	0.0452	0.9212	77.6 ± 0.4[b]	8.79	91.21	0.35
	4.30	0.0323	0.9535	77.5 ± 0.5[b]	8.20	91.80	0.38
	5.00	0.0205	0.9740	76.2 ± 0.6[b]	9.48	90.52	0.49
	6.00	0.0166	0.9906	74.8 ± 0.6[b]	9.52	90.48	0.43
	7.00	0.0094	1.0000	75.7 ± 1.5[b]	8.23	91.77	0.50
Biotite 2a	0.25	0.1001	0.1001	23.6 ± 1.7	73.99	26.01	0.03
	0.32	0.0659	0.1660	58.3 ± 0.8	28.25	71.75	0.02
	0.42	0.1016	0.2677	62.9 ± 1.1	28.02	71.98	0.01
	0.50	0.1249	0.3925	83.0 ± 0.8	10.24	89.76	0.09
	0.70	0.2199	0.6125	86.0 ± 0.7	8.01	91.99	0.01
	0.82	0.0961	0.7085	79.2 ± 0.7	9.87	90.13	0.02
	0.95	0.0667	0.7752	76.5 ± 0.8	12.04	87.96	0.02
	1.12	0.0679	0.8431	73.9 ± 0.9	14.50	85.50	0.02
	1.30	0.0547	0.8979	78.4 ± 0.9	7.96	92.04	0.02
	3.00	0.1021	1.0000	82.1 ± 1.3	6.53	93.47	0.05

Sample	^{39}Ar	$^{40}Ar^{*}/^{39}Ar_K$	Age in Ma	$^{37}Ar_{Ca}/^{39}Ar_K$	$\%^{40}Ar_{atm}$	$\%^{40}Ar^{*}$	$^{40}Ar/^{36}Ar$
Biotite 1a	3.667E-02	13.28 ± 0.03	72.9 ± 0.6	0.11	16.01	83.99	1845.8
Biotite 2a	7.733E-03	13.19 ± 0.06	72.4 ± 0.06	0.02	18.85	81.15	1567.8

J = 0.003104 ± 0.000023.
[a] Power in watts applied to release the argon isotopes.
[b] Fraction plates.

Multiple microfractures in the feldspar porphyroblasts also document the retrograde metamorphism in the Tutak complex.

4.2. The Tutak gneiss dome and Neo-Tethyan Ocean

The aplite is the oldest granite, which belongs to the old continental basement of the Iranian shield (Alizadeh, 2008). It existed long before the Neo-Tethyan Ocean opened and the other granite had been emplaced at the contact between the African-Arabian continent and Iranian microcontinent, within the transpressional tectonic regime (Sarkarinejad et al., 2008; Sarkarinejad and Alizadeh, 2009). Fig. 5 represents the subduction and closing of the Neo-Tethyan Ocean and structural evolution of the Tutak gneiss dome.

According to the proposed model, the sequence of the Tutak complex has deposited on the continental slope that lays to the west of it, before the generation of Neo-Tethys. At the Late Carboniferous, the Paleo-Tethys started subduction (Golonka, 2004) then, by forming of the Neo-Tethyan Ocean, the studied area was upraised and the Surian complex, at the Permian, laid on the Tutak complex unconformably. After final closure of the Paleo-Tethys, the Neo-Tethyan started to subduct underneath Eurasia (Sepehr and Cosgrove, 2004). As the Neo-Tethyan Ocean started to be subducted beneath central Iran at 179.5 ± 1.7 Ma, fore-arc basin sediments, consisting first of sandstones and shales, and then of carbonate rocks that were deposited on top of the older sediments, get metamorphosed. After the subduction and Arabia-central Iran contact at 76.8 ± 0.2 Ma, the new stage of granite invaded the pre-existing facies by emplacement in bivergent wedges (Sarkarinejad and Alizadeh, 2009). By continuous deformation, enhanced heat flow along the Dehbid shear fault system (Surian and Mazayjan) in wrench corridor enabled orogen-

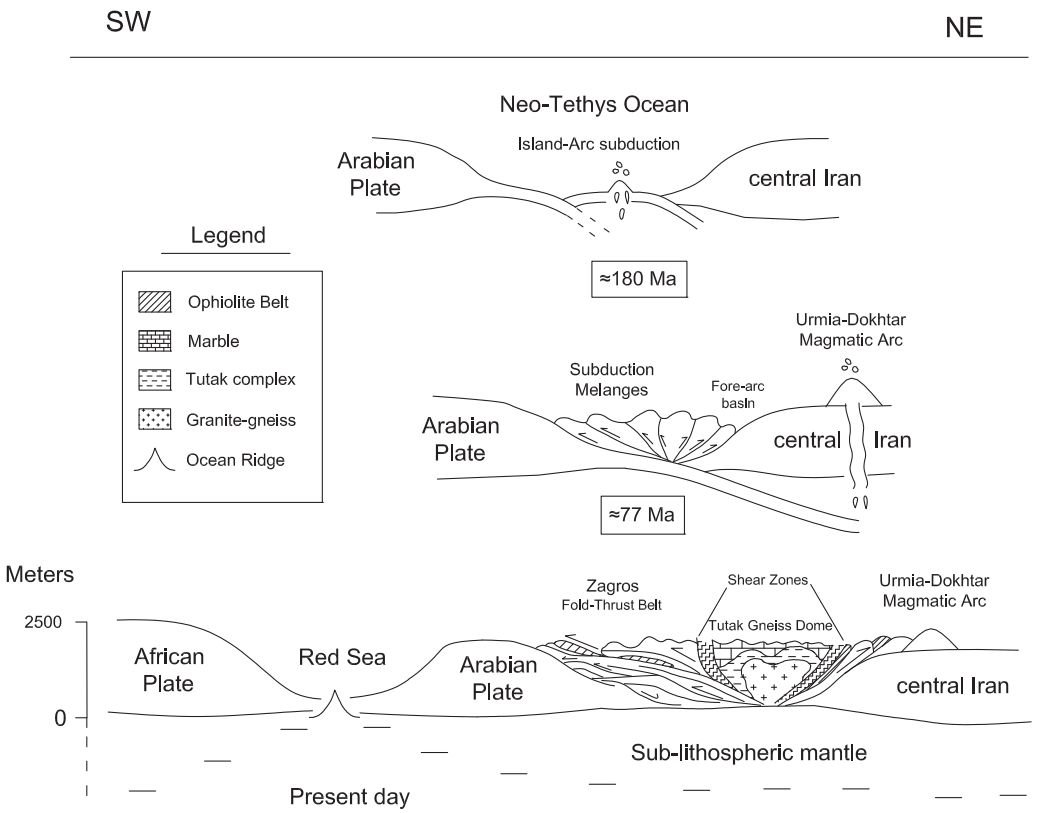

Fig. 5. Succession of events at the origin of the Tutak gneiss dome within the Sanandaj-Sirjan metamorphic belt in the Zagros Orogenic Belt and of the closure of the Neo-Tethyan Ocean.

Fig. 5. Succession d'évènements à l'origine du gneiss de Tutak, au sein de la ceinture métamorphique Sanandaj-Sirjan dans la ceinture orogénique du Zagros, et de la fermeture de l'océan Néo-Téthysien.

parallel extension at NW–SE trend and formation of the syn-compressional plutonism.

The ^{40}Ar-^{39}Ar plateau ages of early generations of biotite from the lower metamorphic melange at Neyriz area (Fig. 1), are 119.95 ± 0.88 Ma and 112.58 ± 0.66 Ma. This Late Aptian age is related to early thrusting and formation of HP-LT metamorphic rocks. The dating of two amphibole samples from the amphibolite yields a weighted mean age of 91.23 ± 0.89 Ma. This Turonian–Cenomanian age suggests a later metamorphic event associated with subduction and obduction of the Neyriz ophiolite and later lateral extrusion of HP–LT metamorphic rocks along the inclined Zagros accretionary prism (Sarkarinejad et al., 2009).

There are two ophiolite belts; the Khoy-Neyriz and Naien-Baft surrounding the studied area (Ghasemi and Talbot, 2006). The first ophiolite belt has been obducted over the synthetic thrust faults aligned in the Zagros Thrust System and the other has been thrusted by forming the back-thrust. The presence of compositionally diverse extrusive rocks (e.g. basaltic andesite and andesite) intercalated with a variety of the Upper Cretaceous sedimentary rocks indicates that the Naien ophiolite has both island arc and intra-oceanic components (Hassanipak and Ghazi, 2000).

The closing of the Neo-Tethyan Ocean develops at various rates in the east and west of Iran (Talebian and Jackson, 2004); so convergence of the Arabian platform and central Iranian microcontinent represents an oblique convergence (without interruption by now). Opening of Red Sea and Gulf of Aden resulted in the rotation of Arabia with respect to Africa (Nubia and Somalia) since 30 Ma (Bonatti, 1987; Guiraud and Bosworth, 1999; Hempton, 1987).

5. Conclusions

The doubly plunging anticline of the Tutak gneiss dome has special petrological units from the interior region in the core to the top: the aplite-granite and Bendenow granite-gneiss, Tutak complex (greenschists, micaschists, hornfels, amphibolites and deformed conglomerates) and thick bedded of marbles that are unconformably, covered by the Surian complex.

Amphibolite-facies rocks in the Tutak complex originally derived from the basic and ultrabasic rocks of the down going metamorphosed oceanic slab and so, exhibit a retrograde metamorphism. Later deformation under greenschist facies conditions resulted in retrogression. Multiple microfractures in the feldspar porphyroblasts

also illustrate the retrograde metamorphism in the Tutak complex.

The structural and geochronological relationships lead us to conclude the following:

- intrusion of the prekinematic aplite-granite into the Silurian and Devonian strata;
- deforming of the aplite-granite into the Tutak complex by the coaxial NE–SW extension along the normal faults at 179.5 ± 1.7 Ma as a result of the first subduction of the Neo-Tethyan Oceanic crust;
- NE–SW compression and shortening which resulted by the continuous subduction of the Neo-Tethyan Oceanic crust at 76.8 ± 0.2 Ma;
- closing of the Neo-Tethyan Ocean and collision between the Arabian continent and Iran microcontinent;
- continuing deformation without interruption by now that has been created since 76.8 ± 0.2 Ma and was largely restricted to the transpression and high proportion of simple shear components relative to the pure shear components along the NE–SW.

Acknowledgements

The authors wish to thank reviewers who critically reviewed the manuscript and made valuable suggestions for its improvement. The support of the Urmia and Shiraz Universities through Ph.D. scholarship for the first author, and facilities provided by the Centro de Investigación Científica y de Educación Superior de Ensenada (CICESE), are gratefully acknowledged. Professor John Fletcher is thanked for his fruitful suggestions and interpretation of the thin sections. M.A. García García and A.S. Rosas Montoya assisted with the mass spectrometry and sample preparation.

References

Alizadeh, A., 2008. Structural evolution of the Tutak Gneiss Dome, Southwest of Iran. Ph.D. Dissertation. Khalil Sarkarinejad, University of Shiraz, Iran.

Alavi, M., 1994. Tectonics of Zagros Orogenic Belt of Iran, new data and interpretation. Tectonophysics 229, 211–238.

Amato, J.M., Wright, J.E., Gans, P.B., Miller, E.L., 1994. Magmatically induced metamorphism and deformation in the Kigluaik gneiss dome, Seward Peninsula Alaska. Tectonics 13, 515–527.

Bonatti, E., 1987. Oceanic evolution, rifting or drifting in the Red Sea? Nature 330, 692–693.

Fletcher, R.C., 1995. 3-Dimensional folding and necking of a power-law layer: are folds cylindrical, and if so, do we understand why? Tectonophysics 247, 65–83, doi:10.1016/0040-1951(95)00021-E.

Getty, S., Gromet, P., 1992. Geochronological constraints on ductile deformation, crustal extension, and doming about a basement-cover boundary, New England Appalachians. Am. J. Sci. 292, 359–397.

Ghasemi, A., Talbot, C.J., 2006. A new tectonic scenario for the Sanandaj–Sirjan Zone (Iran). J. Asian Earth Sci. 26, 683–693.

Golonka, J., 2004. Plate tectonic evolution of the southern margin of Eurasia in the Mesozoic and Cenozoic. Tectonophysics 381, 235–273.

Guiraud, R., Bosworth, W., 1999. Phanerozoic geodynamic evolution of northeastern Africa and the northwestern Arabian platform. Tectonophysics 315, 73–108.

Hassanipak, A.A., Ghazi, A.M., 2000. Petrology, geochemistry and tectonic setting of the Khoy ophiolite Northwest Iran. J. Asian Earth Sci. 18, 109–121.

Hempton, M.R., 1987. Constraints on Arabian plate motion and extensional history of the Red Sea. Tectonics 6, 687–705.

Houshmand-Zadeh, A., Sheile, M., Hamdi, B., 1990. Explanatory text of the Eqlid Quadrangle map, Geological Survey of Iran, Ministry of mines and metals. Geological quadrangle, No. G 10, scale 1 25000.

Mohajjel, M., Fergusson, C.L., Sahandi, M.R., 2003. Cretaceous–Tertiary convergence and continental collision, Sanandaj–Sirjan Zone, western Iran. J. Asian Earth Sci. 21, 397–412.

Nuri, K, 2005. Investigation of the genesis of Bendenow granite-gneiss with Tutak metamorphic complex, Eastern Bavanat. Ph.D thesis, Azad University of Iran.

Ramsay, J.G., 1967. Folding and fracturing of rocks. McGraw-Hill, New York.

Sarkarinejad, K., 2007. Quantitative finite strain and kinematic flow analyses along the Zagros transpression zone Iran. Tectonophysics 442, 49–65.

Sarkarinejad, K., Faghih, A., Grasemann, B., 2008. Transpressional deformations within the Sanandaj-Sirjan metamorphic belt (Zagros Mountains, Iran). J Structural Geol. 30, 818–826.

Sarkarinejad, K., Alizadeh, A., 2009. Dynamic model for the exhumation of the Tutak gneiss dome within the bivergent wedges in the Zagros Thrust System of Iran. J. Geodynamics 47, 201–209.

Sarkarinejad, K., Azizi, A., 2008. Slip partitioning and inclined dextral transpression along the Zagros Thrust System, Iran. J. Structural Geol. 30, 116–136.

Sarkarinejad, k., Laurent, G., Faghih, A., 2009. Kinematic vorticity flow analysis and ^{40}Ar-^{39}Ar geochronology related to inclined extrusion of the HP–LT metamorphic rocks along the Zagros accretionary prism, Iran. Journal of Structural Geology 31, 691–706.

Schneider, D.A., Zeitler, P.K., Kidd, W.S.F., Edwards, M.A., 2001. Geochronologic and constrains on the tectonic evolution and exhumation of Nanga-Parbat, Western Himalaya Syntaxis, Revisited. J. Geol. 109, 563–583.

Sepehr, M., Cosgrove, J.W., 2004. Structural framework of the Zagros Fold-Thrust Belt Iran. Marine and Petroleum Geology 21, 829–843.

Steiger, R.H., Jäger, E., 1977. Subcommission on Geochronology: convention on the use of decay constants in Geo and Cosmochronology. Earth Planet. Sci. Lett. 36, 359–362.

Stocklin, J., 1968. Structural history and tectonics of Iran: a review. AAPG Bull. 52, 1229–1258.

Talebian, M., Jackson, J., 2004. A Reappraisal of earthquakes focal mechanisms and active shortening in the Zagros mountains of Iran. Geophys. J. Int. 156, 506–526.

Teyssier, C., Whitney, D.L., 2002. Thermal and Mechanical Significance of Gneiss dome in the Evolution of Orogens, Colorado Convention Center. 2002 Denver Annual Meeting (October 27–30, 2002): decompression of subducted continental crust and partial melting of orogens, Paper No 50–57.

Whittington, A.G., 2004. The exhumation of gneiss domes in bivergent wedges: Geometrical concepts and examples from the Himalayan syntaxes. In: Whitney, D.L, Teyssier, C., and Siddoway, C.S., Gneiss domes in orogeny. Geological Society of America, Special Paper 380.

York, D., Evensen, N.M., López Martínez, M., De Basabe Delgado, J., 2004. Unified equations for the slope, intercept and standard errors of the best straight line. Am. J. Phys. 72 (3), 367–375.